ACS OMEGA

http://pubs.acs.org/journal/acsodf

Article

Effect of Physical Nature (Intact and Powder) of Coal on CO_2 Adsorption at the Subcritical Pressure Range (up to 6.4 MPa at 298.15 K)

Maram Almolliyeh,* Snehasis Tripathy, Sivachidambaram Sadasivam, Shakil Masum, and Hywel Rhys Thomas

Cite This: https://doi.org/10.1021/acsomega.2c07940

Read Online

ACCESS | Metrics & More | Article Recommendations

ABSTRACT: This study examines the influence of subcritical pressure and the physical nature (intact and powder) of coal samples on CO_2 adsorption capacity and kinetics in the context of CO_2 sequestration in shallow level coal seams. Manometric adsorption experiments were carried out on two anthracite and one bituminous coal samples. Isothermal adsorption experiments were carried out at 298.15 K in two pressure ranges: less than 6.1 MPa and up to 6.4 MPa relevant to gas/liquid adsorption. The adsorption isotherms of intact anthracite and bituminous samples were compared to that of the powdered samples. The powdered samples of the anthracitic samples had a higher adsorption than that of intact samples due to the exposed adsorption sites. The intact and powdered samples of bituminous coal, on the other hand, exhibited comparable adsorption capacities. The comparable adsorption capacity is attributed to the intact samples' channel-like pores and microfractures, where high density CO_2 adsorption occurs. The adsorption−desorption hysteresis patterns and the residual amount of CO_2 trapped in the pores reinforce the influence of the physical nature of the sample and pressure range on the CO_2 adsorption−desorption behavior. The intact 18 ft AB samples showed significantly different adsorption isotherm pattern to that of powdered samples for experiments conducted up to 6.4 MPa equilibrium pressure due to the high-density CO_2 adsorbed phase in the intact samples. The adsorption experimental data fit into the theoretical models showed that the BET model fit better than the Langmuir model. The experimental data fit into the pseudo first order, second order, and Bangham pore diffusion kinetic models showed that the rate-determining steps are bulk pore diffusion and surface interaction. Generally, the results obtained from the study demonstrated the significance of conducting experiments with large, intact core samples pertinent to CO_2 sequestration in shallow coal seams.

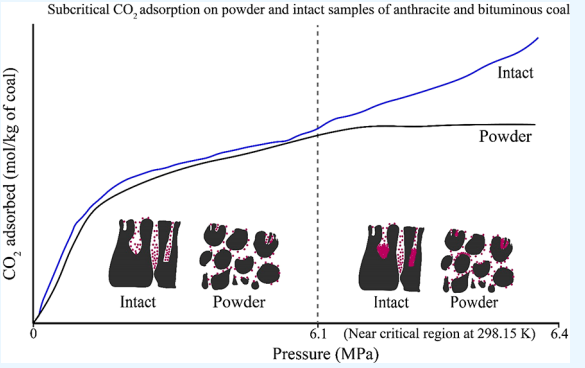

Downloaded via CARDIFF UNIV on February 10, 2023 at 12:41:38 (UTC).
See https://pubs.acs.org/sharingguidelines for options on how to legitimately share published articles.

1. INTRODUCTION

Geological carbon dioxide (CO_2) storage, especially, sequestration in unmineable coal seams, has a high potential owing to higher CO_2 storage capacity.[1,2] Numerous experimental studies have revealed that coal can adsorb and store CO_2, and coal seams have the potential to store 300−964 Gt CO_2 globally.[1−6] CO_2 storage capacity of coal seams are estimated by considering the experimentally determined adsorption capacity of the various coal ranks as one of the factors.[1] However, the knowledge gap in the effect of sample physical type (intact or powdered) and subcritical pressure range (liquid and gas) on CO_2 adsorption must be improved in order to comprehend the storage potential of the shallow level coal seams.

Adsorption capacity and kinetics of CO_2 adsorption on coal samples are often related to coal rank, moisture content, swelling characteristics, porosity, temperature, and operating pressures.[1,7−9] In general, the CO_2 adsorption capacity of a specific rank of coal increases with pressure and showed decreasing trend in a few studies.[10−15] To maximize storage capacity and safety, supercritical CO_2 injection into coal seams deeper than 500 m has been considered. However, at greater depths, the confining pressure and coal swelling influence the permeability of high-density CO_2 and hinder the storage potential.[16] As a consequence, CO_2 storage at shallower depth coal deposits has received attention, and horizontal injection of subcritical CO_2 in existing shallow level coal mines has been regarded as a technological advance because it improves the CO_2 contact area while reducing the impact of coal swelling.[17] CO_2 adsorption is a

Received: December 13, 2022
Accepted: February 1, 2023

ACS Publications

© XXXX The Authors. Published by American Chemical Society

gas/liquid phase adsorption at coal seam depths where the temperature and pressure values are less than the critical value (31 °C and 7.38 MP).[18−21] The density of CO_2 is extremely sensitive near the critical point (van der Waals loop region) where the coexistence of liquid and vapor phases would influence the way coal-CO_2 interaction occurs in general.[14,22]

Adsorption capacity and kinetics data on intact coal samples are limited for the subcritical range[20,23−25] due to the difficulties with core sample extraction, extended time needed to achieve equilibrium, variable permeability, and pore diffusion/condensation.[24] Moreover, pulverizing coal samples can alter or lose their physical nature, which affects their CO_2 adsorption properties.[26−28] Consequently, it stands to reason that comparing the CO_2 adsorption capacity of intact and powdered samples of various coal ranks would reveal the effect of the sample's physical type on CO_2 adsorption. Therefore, more laboratory investigations with intact coal samples at subcritical temperature and pressure region are fundamental to understanding coal-CO_2 interactions.

Methane desorption was widely focused on in previous works,[29−31] the CO_2 desorption data are less discussed in the literature, and it is important to investigate the reversibility of pore trapped CO_2. The pore trapping mechanisms such as pore blockage, gas cavitation, adsorption induced deformation, and pore network (ink bottle effect) affect the adsorption−desorption hysteresis pattern and correlate with the coal rank.[32] In general, a limited number of studies modeled the desorption kinetics.[32,33] Among the two dominant kinetic models, pseudo-first order (PFO) and pseudo-second order (PSO), the PSO model agreed well with the experimental results obtained using a manometric adsorption experimental set up for an intact and powdered bituminous coal sample, implying that CO_2 adsorption kinetics and hysteresis were determined by pore diffusion and condensation.[34,35] Njikam and Schiewer (2012)[36] modified the commonly used adsorption kinetic models (PFO and PSO) to adopt the desorption process. These models have not been fully explored for CO_2 adsorption−desorption.[23] The rate-determining steps for the adsorption−desorption process can be predicted by fitting the adsorption−desorption kinetics experimental data in the Bangham pore diffusion model and the modified PFO and PSO equations.[36,37]

While efforts have been made to understand supercritical CO_2 adsorption on powdered samples, the present study seeks to investigate the CO_2 adsorption capacity and kinetics of intact anthracite and bituminous coal samples in comparison to powdered samples, how the adsorption−desorption isotherm hysteresis differs for powder and intact samples in terms of the physical type of coal, and the effects of subcritical and the near critical injection pressure range at 298 K. For this, a manometric gas adsorption experimental setup was employed. The results of adsorption studies utilizing intact and powdered samples of two anthracite coals and a bituminous coal were fitted into theoretical isotherm and kinetic models to determine the CO_2 adsorption mechanism at 298.15 K.

2. MATERIALS AND METHODS

2.1. Coal Properties and Sample Preparation. Coal samples were collected from two coal mines in South Wales Coalfield, Wales, UK. The anthracite coal samples were obtained from the Aberpergwm coal mine (51°44′28.8″N 3°38′36.0″W), while the bituminous coal (water content 0.96%) samples were obtained from the Big Pit National Museum (51.7724°N 3.1050°W). Coal blocks were extracted from the Aberpergwm colliery's two coal seams, the 9 ft seam (with a water content of 0.91%) at a depth of 550 m and the 18 ft seam (water content 0.78%) at a depth of 500 m. The Big Pit coal had a water content of 0.96% and was extracted from a coal seam at a depth of 90 m. These samples will be referred to as 9 ft AB and 18 ft AB and BP hereafter.

The proximate and ultimate analyses were conducted in accordance with the British Standards Institution (BSI) and American Society for Testing Materials (ASTM) standards.[38−43] Table 1 summarizes the analyses. On the basis of carbon content, volatiles, and gross calorific value, the Aberpergwm samples (9 ft AB and 18 ft AB) were classified as anthracite coal (high rank). The Big Pit (BP) sample was identified as low volatile bituminous coal based on their carbon content.[44,45]

Table 1. Proximate and Ultimate Analysis of the Coal Samples Investigated in This Study

analytical		18 ft AB	9 ft AB	BP
Proximate analysis				
Water Content	% mass	0.78	0.91	0.96
Ash Content	% mass	1.38	4.62	12.7
Volatiles content	% mass	5.08	5.73	29
Calorimetry				
High calorific value	MJ/kg	35.04	35.60	33.68
Low calorific value	MJ/kg	34.30	32.89	-
Ultimate analysis				
Total Carbon	% mass	92.05	89.5	83.87
Total sulfur	% mass	0.73	0.87	1.62
Total hydrogen	% mass	3.31	3.16	-
Nitrogen	% mass	1.27	1.31	3.3
Oxygen	% mass	0.5	0.33	-

2.2. Intact and Powdered Sample Preparation and SEM Imaging. Coal cores were drilled from large coal blocks using a core drill machine equipped with a diamond saw-tipped core drilling bit with a 50 mm internal diameter. Samples were air-dried prior to conducting adsorption experiments. Figure 1 illustrates the coal core sample and powdered sample. To prepare powdered samples, coal chunks were pulverized and passed through a 63 μm-mesh screen.

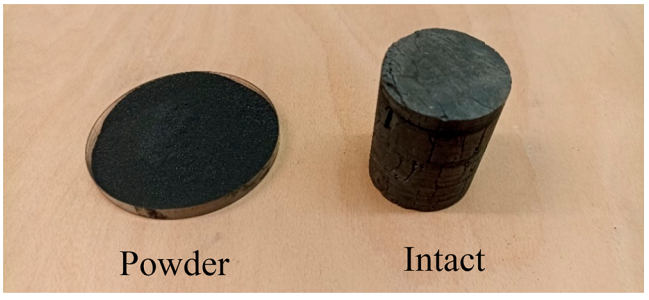

Figure 1. Photographs of coal core and powdered samples.

The SEM images of the intact and powdered coal samples were obtained using a Zeiss Sigma HD field emission gun analytical high-resolution SEM (natural samples). The samples were finely gold coated to reduce the charging effect, and the images were used to visualize the structural change in the powder and intact samples of relevant coal rank, as discussed in section 4.1.

https://doi.org/10.1021/acsomega.2c07940
ACS Omega XXXX, XXX, XXX−XXX

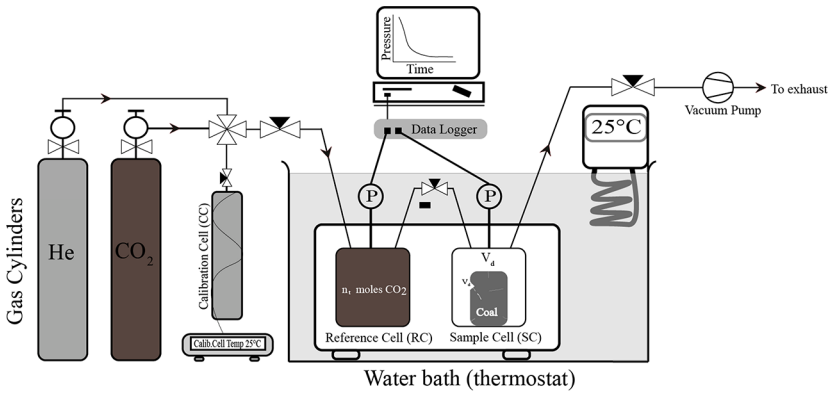

(a)

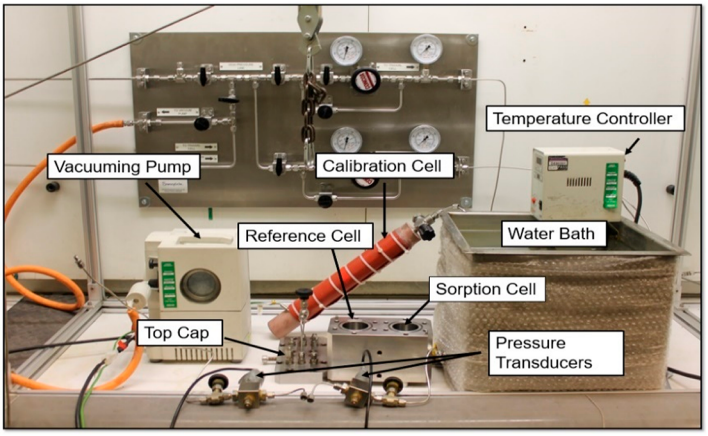

(b)

Figure 2. (a) Schematic of the manometric adsorption experimental setup and (b) a photograph of the main components of the manometric adsorption set up.

2.3. Methodology. A manometric adsorption apparatus (volumetric) was used in this study. The apparatus was supplied by GDS Instruments, UK. It is capable of operating at pressures up to 20 MPa and temperatures up to 338 K (65 °C). Schematic of the manometric sorption apparatus and experimental setup is presented in Figure 2a, and a photograph of the major components is presented in Figure 2b. The test setup instrumentation is as follows: (1) a manometric unit consisting of a reference cell (RC) for storing a known quantity of gas and a sample cell (SC) for storing the adsorbent, (2) needle valves for connecting and isolating the RC and SC, (3) pressure transducers with a resolution of 0.002 MPa (2 kPa) and accuracy of 0.15%, and data loggers, (4) a water bath with a temperature controller for maintaining the temperature of 298.15 K ± 0.01 K, and (5) A calibration cell (volume = 0.0004892 m^3) that determines the empty and sample loaded void volumes of RC and SC using the helium pycnometry (He-pycnometry) method. The calibration cell heater is kept at a constant temperature of 298.15 K ± 0.01.

Manometric adsorption is a mass balance technique that utilizes precise pressure, volume, and temperature measurements.[46] The experimental concept is as follows: (i) determine void volumes (v_d) of RC and SC using the He-pycnometry method, (ii) prepare a known quantity of CO_2 gas in RC and expand it into SC while monitoring the pressure drop; repeat the procedure progressively by increasing pressure in RC; and (iii) calculate the adsorbed amount using an appropriate equation of state (EoS) for CO_2 and the perfect gas law.

The He-pycnometry method, which involves injecting He into the adsorption cell at experimental ambient temperature and pressure, can be used to approximate the void volume (v_d) available for gas molecules in the adsorption cell. The void volume (v_d) is calculated via the He-pycnometry method and using the perfect gas law as[46−50]

$$v_d = \frac{n_{He} RTZ_{He}}{P_{He}} \quad (1)$$

where n_{He} is the number of moles of He injected (mol), P_{He} is the pressure of He (Pa), T is the absolute temperature (298.15 K), and R is the gas constant (8.314 J/mol·K). The compressibility factor (Z_{He}) values were calculated using the Peng−Robinson equation of state (PR-EoS).[22]

The amount of CO_2 adsorbed or desorbed is calculated as follows:[46−49]

$$n_t^{CO_2} = \frac{p_{rc+sc}^{CO_2}}{RTZ_{(p,v)}} v_d \quad (2)$$

$$n_e^{CO_2} = \frac{p_{eq}^{CO_2}}{RTZ_{(p,v)}} v_d \quad (3)$$

https://doi.org/10.1021/acsomega.2c07940
ACS Omega XXXX, XXX, XXX−XXX

Table 2. Experimental Program of CO_2 Adsorption and Desorption Tests Conducted in This Study[a]

	coal sample/location	9 ft AB		18 ft AB		BP	
pressure range	sample description	powder	intact	powder	intact	powder	intact
subcritical pressure (<6.1 MPa)	Adsorption test	√	√	√	√	√	√
	Desorption test	-	√	√	√	-	-
up to near-critical pressure (6.1−6.5 MPa)	Adsorption test	-	-	√	√	-	-
	Desorption test	-	-	√	√	-	-

[a]The tick mark represents the experiments conducted.

$$n_{ad}^{CO_2} = \frac{n_t^{CO_2} - n_e^{CO_2}}{m_s} \text{ for adsorption} \quad (4)$$

$$n_{de}^{CO_2} = \frac{n_e^{CO_2} - n_t^{CO_2}}{m_s} \text{ for desorption} \quad (5)$$

where $n_{ad/de}^{CO_2}$ is the number of moles of CO_2 adsorbed during adsorption (ad) and desorption (de) (mol; 44.01 g of CO_2/mol), $n_t^{CO_2}$ is the known amount of CO_2 present in the gas phase (RC + SC) at the beginning of the adsorption or desorption experiment (mol), $n_e^{CO_2}$ amount of CO_2 present in the gas phase (RC + SC) at the equilibrium (end of the adsorption or desorption test) (mol), v_d is the void volume available for gas (m^3), $p_{rc+sc}^{CO_2}$ is the initial CO_2 pressure in RC and SC before adsorption, $p_{eq}^{CO_2}$ is the equilibrium pressure of CO_2 in RC and SC after adsorption (Pa), Z is the compressibility factor of CO_2, and R is the universal gas constant (R = 8.314 Pa m^3/K/mol). $n_t^{CO_2}$ is the known amount of CO_2 present in the gas phase (RC + SC) at the beginning of the adsorption experiment (mol).

In this study, the adsorption experiments were conducted by increasing the CO_2 pressure in stages, starting at 0.5 MPa until it reached to a maximum target pressure of 6.5 MPa pressure. CO_2 desorption experiments were conducted using a pressure step-down procedure from the peak equilibrium pressure to the null pressure. Changes in gas phase pressure were recorded every 10 s to capture the rapid rate of adsorption−desorption at the beginning of the experiment and used to determine the adsorption capacity and kinetics. The experimental program is summarized in Table 2.

The van der Waals loop occurs near the critical pressure range (6.1 to 6.4 MPa at 298.15 K), in which liquid and vapor CO_2 coexist and differ in molar volumes. The CO_2 critical pressure value is 6.4 MPa at 298.15 K.[51] Above this point, the coexistence of liquid and vapor is impossible. This is a key technical aspect that affects adsorption results as an overestimation or underestimation of CO_2 excess adsorption calculations. To overcome this phenomenon, the following theoretical consideration was made in the current study to calculate the amount of CO_2 adsorbed in the near critical region (6.1 MPa to 6.4 MPa at 298.15 K). When the vapor and liquid phase is in equilibrium, the chemical potential and Gibbs free energy of both phases are equal for pure fluids, and they are thermally and physically in equilibrium. The calculated molar volumes of liquid (n_L) and vapor (n_v) phases by PR-EoS at a given temperature and pressure were used to calculate the volume fraction (v^F) of vapor phase CO_2 following:[22,52]

$$v^F = \frac{n_v}{n_v + n_L} \quad (6)$$

where n_L and n_v are the molar volumes of liquid and vapor phases, respectively, and they are calculated using PR-EoS for a given pressure and temperature. The volume fraction ratio of vapor (v^F) and liquid CO_2 was used to calculate the total number of moles injected at near critical phase region (6.1 MPa to 6.4 MPa at 298.15 K).

3. THEORY

3.1. Evaluation of CO_2 Adsorption by Langmuir and BET Isotherm Models. The nonlinear form of the Langmuir isotherm model is expressed as[47,53−55]

$$m_{eq} = m_\infty \frac{bP_{eq}}{1 + bP_{eq}} \quad (7)$$

where P_{eq} is equilibrium pressure (Pa), m_{eq} is the mass of CO_2 adsorbed at given equilibrium pressure (g/kg), m_∞ is limiting value of mass adsorbed (maximum adsorption capacity), also mass of a maximum monolayer adsorbate covering the surface of the sorbent (g/kg), and b is the Langmuir parameter, which is also reciprocal of half-loading pressure, (Pa^{-1}). In this study, m_∞ and b values were obtained from nonlinear regression analysis.

The thermodynamic parameters, e.g., energy of adsorption and Gibbs free energy were calculated from the Langmuir parameters (m_∞ and b) as[56−58]

$$b = b_0 \exp\left(\frac{-\Delta H_{ad}}{RT}\right) \quad (8)$$

$$b_0 = \frac{N_m \sigma_A \tau_0}{\sqrt{2\pi MRT}} \quad (9)$$

where b_0 is the exponential factor (Pa^{-1}), ΔH_{ad} is energy of adsorption (J/mol), τ_0 is vibration period related to the residence time of the adsorbed CO_2 molecule (typically on the order of 10^{-13} s), N_m is the number of molecules adsorbed (related to m_∞ and Avogadro's number), σ_A is cross sectional area covered by one CO_2 molecule (m^2), M is molecular mass of CO_2 (0.04401 kg/mol).

The Gibbs free energy (ΔG_{ad}^0, kJ/mol) can be calculated as[56]

$$\Delta G_{ad}^0 = -RT \ln b^{-1} \quad (10)$$

The nonlinear form of the BET model is expressed as[59]

$$n = \frac{n_{mon} c \frac{P_{eq}}{P_0}}{\left(1 - \frac{P_{eq}}{P_0}\right)\left[1 - (1 - c)\frac{P_{eq}}{P_0}\right]} \quad (11)$$

where n is the amount of gas adsorbed (mol), n_{mon} is number of moles to cover monolayer adsorption (mol), P_{eq} is the equilibrium pressure (Pa), P_0 is the saturation pressure (7.39×10^6 Pa), c is dimensionless parameter related to energy of adsorption ΔH_{ad}. The c and n_{mon} values were obtained from nonlinear regression analysis. The dimensionless parameter c is related to the adsorption energy and is defined as[59]

https://doi.org/10.1021/acsomega.2c07940
ACS Omega XXXX, XXX, XXX−XXX

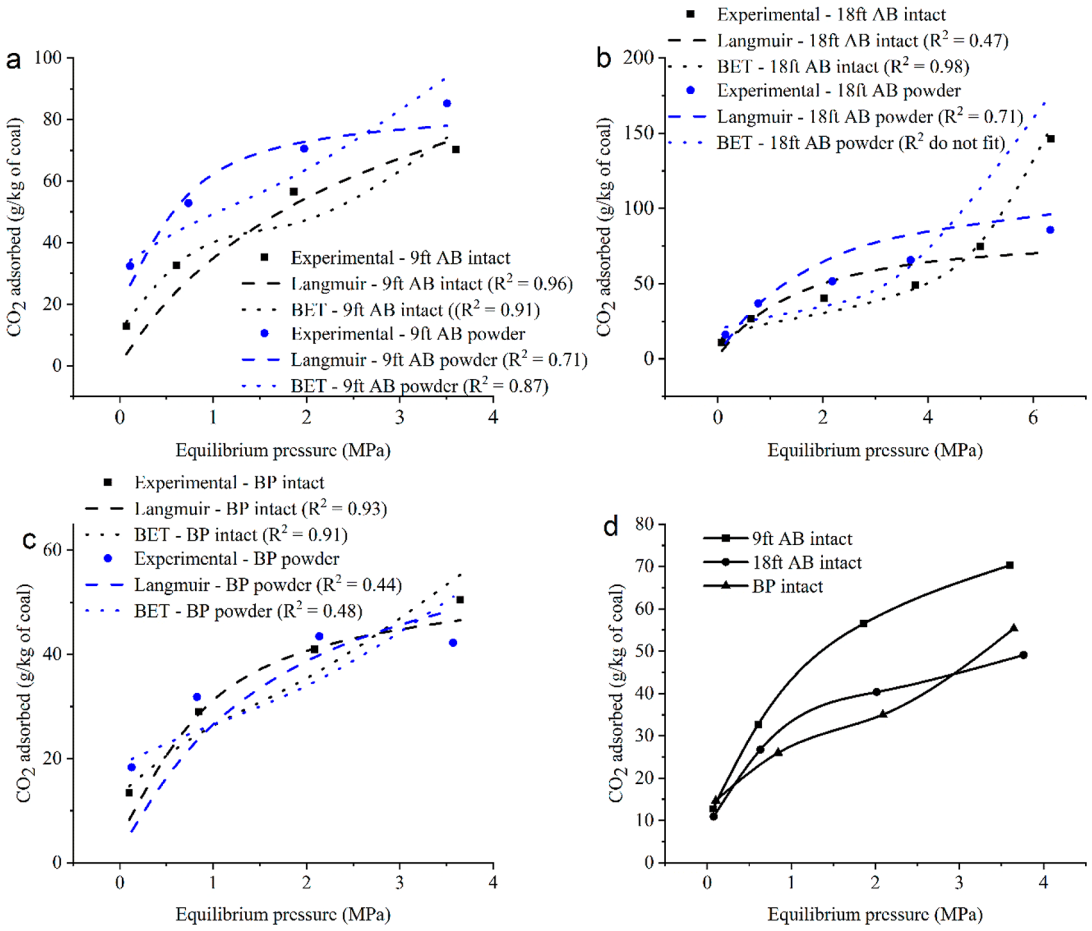

Figure 3. Experimental, Langmuir, and BET CO_2 adsorption isotherms of (a) 9 ft Aberpergwm coal samples (powder and intact), (b) 18 ft Aberpergwm coal samples (powder and intact), (c) CO_2 Big Pit coal (powder and intact), and (d) comparison of intact samples of 9 ft Aberpergwm, 18 ft Aberpergwm, and Big Pit coal.

$$c \approx e^{[Q_1 - Q_2/RT]} \tag{12}$$

where Q_1 is the adsorption energy on a bare surface (monolayer adsorption) (J/mol), and Q_2 is the energy of second and subsequent layers (J/mol).

The surface area of 1 mol of CO_2 in the liquid state is calculated as[60,61]

$$a_s = 1.091(V_m^L)^{2/3} \tag{13}$$

$$A_s = a_s \times n_{mon} \tag{14}$$

where a_s is effective surface area covered by 1 mol of CO_2 (m^2/mol), and V_m^L is liquid molar volume of CO_2 (m^3/mol). The number 1.091 is the packing factor of 12 neighboring molecules in a bulk liquid and six on a plane.[60] A_s is the specific surface area (m^2/kg), and n_{mon} is number of moles required to complete the monolayer coverage per kg of coal sample, mol/kg.

3.2. Adsorption−Desorption Kinetics. The data obtained from the experimental program (Table 2) were fitted into pseudo-first-order (PSO) and pseudo-second-order rate equations.[62,63]

$$\text{PFO: } q_t = q_e(1 - e^{(-kt)}) \tag{15}$$

$$\text{PSO: } q_t = \frac{t}{\frac{1}{q_e}t + \frac{1}{k_{a2}q_e^2}} \tag{16}$$

where q_t represents the mass of CO_2 adsorbed per unit mass of adsorbent at time t (g of CO_2/kg of coal), q_e represents the mass CO_2 adsorbed per unit mass of adsorbent at equilibrium (g of CO_2/kg of coal), k is the first-order rate constant (h^{-1}), and k_2 is the second-order rate constants (kg g^{-1} h^{-1}).

Desorption kinetics data were fitted into modified PFO and PSO equations. The equations are modified on the basis that the amount of CO_2 adsorbed on coal is the rate determining factor.[36]

$$\text{PFO: } q_t = q_e/e^{(k_{d1}t)} \tag{17}$$

$$\text{PSO: } q_t = \frac{q_e}{1 + (k_{d2}q_e t)} \tag{18}$$

where k_{d1} is the first-order rate constant for desorption, (h^{-1}) and k_{d2} is the second-order rate constants for desorption (kg g^{-1} h^{-1}).

To predict the influence of pore diffusion mechanism of coal-CO_2 interaction, experimental data were also fitted into the Bangham model.[64−66]

$$q_t = q_e(1 - \exp(-k_b t^n)) \tag{19}$$

where k_b (h^{-1}) and n are constants of the model.

https://doi.org/10.1021/acsomega.2c07940
ACS Omega XXXX, XXX, XXX−XXX

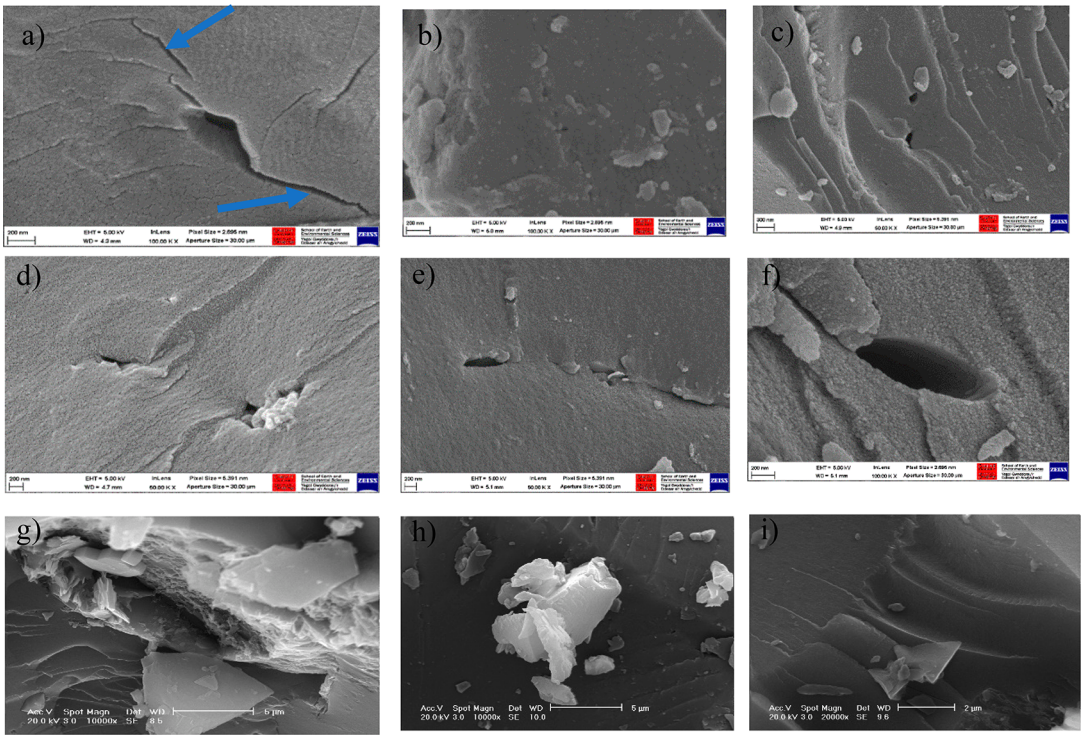

Figure 4. SEM images of a) BP bituminous intact coal, b, c) BP bituminous powder coal, d) 18 ft AB anthracite intact coal, e and f) 18 ft AB anthracite powder coal, and g) 9 ft AB anthracite intact coal, h) and i) 9 ft AB anthracite powder coal.

4. RESULTS AND DISCUSSION

4.1. Adsorption Capacity of Intact and Powdered Coals at Subcritical and near Critical Conditions. Adsorption behavior of powder and intact samples of two different ranks are compared here. The adsorption isotherms of 9 ft AB, 18 ft AB, and BP coal samples are presented in Figure 3(a), (b), and (c), respectively for the maximum CO_2 injection pressure up to 6.4 MPa, which is below the critical pressure of CO_2 at 298.15 K. The powder samples of 9 and 18 ft AB anthracite coal exhibited greater CO_2 adsorption than the intact samples (Figure 3a,b). In contrast, the intact bituminous sample of Big Pit coal exhibited similar adsorption behavior to that of the powder sample (Figure 3c). All the three intact coal samples showed similar adsorption isotherm pattern with 9 ft AB showing slightly higher adsorption capacity (Figure 3d).

The adsorption capacities of powder samples of the 9 and 18 ft AB coal were about 21% and 36% higher than that of intact samples, respectively. The results show that more adsorption sites are available in the powdered samples compared with the intact samples. The case is different when comparing powder and intact for bituminous BP samples. The CO_2 adsorption isotherm pattern of the intact sample was similar to that of powdered samples for experiments conducted up to equilibrium pressures of 3.6 MPa (Figure 3c). Similar behavior for bituminous coal has been reported by Pone et al. (2009),[67] where the adsorption capacity of powdered sample was 14% lower than the intact sample at applied pressure of 3.1 MPa. Zhao et al. (2014)[68] reported that bituminous coal has channel-like and interconnected pores. Such pore structures are observed for both high- and low-volatile bituminous coals. Xu et al. (2015)[26] and Tan et al. (2018)[27] suggested that during the sample grinding process, powdered samples lost most of the channel-like fracture network and pore entrance. The porous matrix difference between the intact and powdered samples resulted in comparable adsorption capacities for the bituminous coal.

This analysis indicated that the sample physical nature has an impact on the CO_2 adsorption on coal samples. To visualize the changes in sample structure, the SEM images of the powdered coal samples and intact samples were taken to identify the nano-/micropores. Figure 4 presents the SEM images for BP and 18 ft AB intact and powdered samples. The nanosized channel like pore entrance/fractures are clearly visible in the intact specimens of the bituminous sample (Figure 4a). However, the channel like pore openings have not been identified in the powdered bituminous BP sample indicating the pulverization of the sample destroys them (Figure 4b,c). The features of intact bituminous sample have not been identified in anthracite intact samples (Figure 4d). The anthracite 18 ft AB powdered samples showed the exposed nanosized pore entrances (Figure 4e,f) which were observed in intact samples as well. Similarly, no discernible differences were found between anthracite 9 ft AB intact and powdered samples (Figure 4g–i). These results are consistent with the adsorption isotherm pattern observed for the intact and powdered samples of the bituminous and anthracite coal samples. As discussed elsewhere, the high-density CO_2 adsorption in channel-like pores of the intact bituminous coal reflected the adsorption capacity (Figure 3).

The results from the adsorption tests and SEM images clearly showed that the powdered and intact samples of coals considered in this investigation exhibited different adsorption capacities. Therefore, testing intact samples is more appropriate for determining the adsorption capacity since it reflects the fabric and structure of in situ coal seam.

The injection pressure is considered as one of the key parameters that affects the adsorption capacity of coals. For pressures lower than 6.1 MPa, only the gas phase would exist in the system. At higher pressures, that is, near the critical region

https://doi.org/10.1021/acsomega.2c07940
ACS Omega XXXX, XXX, XXX−XXX

(6.1 to 6.4 MPa), the coexistence of liquid and vapor phases of CO_2 is evident. The fraction of liquid and gas CO_2 coexisted during the injection were calculated as described in section 2.3.

The adsorption isotherms of 18 ft AB powder and intact coal for an injection pressure range of 0.5 to 6.4 MPa are presented in Figure 3b. It can be seen from Figure 3b that the 18 ft AB intact specimen showed maximum capacity of 3.328 mol of CO_2/kg of coal (146 g/kg), and the powdered specimen exhibited 1.843 mol of CO_2/kg of coal (52.12 g/kg). It is noted that, at lower pressures (<6.1 MPa), the powdered sample showed a higher adsorption capacity than the intact sample. However, at a near critical injection pressure range (6.1 to 6.4 MPa), the intact sample showed a higher adsorption capacity than the powder. This is because the condensation and high-density CO_2 adsorption occur in the nanopores and microfractures of intact samples due to the gas cavitation or condensation.

4.2. Isotherm Modeling Results. *4.2.1. Evaluation of CO_2 Adsorption on Coal Using the Langmuir Model.* To validate the model, the CO_2 adsorption equilibrium data from the experiments were fitted with the mathematical expression of the Langmuir model using nonlinear regression analysis (eq 7) and are shown in Figure 3a−c and Table 3. Figure 3a−c shows the plots comparing the experimental data of intact and powdered samples of 9 ft AB, 18 ft AB, and BP against results obtained from the Langmuir model. Table 3 summarizes the Langmuir parameters.

Table 3. Langmuir Parameters, b - Half-Loading Pressure, and m_∞ - Maximum Adsorption Capacity, Obtained from Plots (Figure 3)

sample description	half-loading parameter b, Pa^{-1}	maximum adsorption capacity, m_∞, g of CO_2/kg of coal	R^2 and (standard error of estimate)
AB 18 ft intact	8.50×10^{-7}	84.00	0.47 (32)
AB 18 ft powder	6.61×10^{-7}	119.00	0.71 (13)
AB 9 ft intact	1.56×10^{-6}	80.54	0.96 (4.5)
AB 9 ft powder	2.49×10^{-6}	91.77	0.71 (10.6)
Big Pit intact	1.80×10^{-6}	53.66	0.93 (4.1)
Big Pit powder	4.29×10^{-6}	45.57	0.44 (7.5)

At lower and intermediate pressures (<6.1 MPa), there was good agreement between experimental and model results (Figure 3a,c). The experimental results deviated from the model to show the multilayer build-up at high pressures (from 6.1 to 6.4 MPa). This was evident in the intact and powdered samples of 18 ft AB (Figure 3b). These findings support the expected theory of high-density CO_2 adsorption in microporous structure of the intact samples at elevated pressures.

It was explained in the previous section why the bituminous intact coal sample had a similar adsorption capacity as the powdered sample of the same coal, which was reflected in the calculated maximum capacity. The predicted Langmuir maximum adsorption capacity for the BP intact (bituminous) was 53.66 g of CO_2/kg of coal, while the powdered BP sample was 45.57 g of CO_2/kg of coal. The inverse of half-loading pressure of all the samples (Langmuir parameter b, Pa^{-1}), the predicted pressure at which half of the maximum adsorption capacity can be achieved, ranged from 10^{-6} to 10^{-7} Pa^{-1} (Table 5).

Half-loading pressure is an important economic parameter in coal seam CO_2 storage.[69] Conducting an isobaric adsorption experiment at the half-loading pressure value predicted by the Langmuir model can yield half of the maximum adsorption capacity of the specific coal sample. Experiments at 1.59 MPa (half-loading pressure; reciprocal of the b-value for 18 ft AB intact) can, for example, achieve a loading of half the 86.97 g CO_2/kg of coal (Figure 3b; Table 3). Similarly, at 0.40 MPa (inverse of the b value for 9 ft AB intact; Figure 3a; Table 3), half of 80.54 g of CO_2/kg of coal can be loaded.

The observations discussed above imply that the monolayer was covered at pressures less than 1 MPa, and the isotherm pattern observed at intermediate pressures showed the type II isotherm slope[70] rather than the plateau typically observed in Langmuir type adsorption, representing the multilayer build-up that occurs at coal surfaces.[60] The pattern was visible in the intact coal samples because capillary condensation occurs in the pores of the intact samples, and the plots in Figure 3a−c showed a deviating uptrend from the Langmuir model.

The adsorption energy (ΔH_{ad}) was calculated using the Langmuir parameters obtained from the isotherm model fittings (maximum Langmuir adsorption capacity (m_∞) and the constant b). The energy of adsorption values was between −15 kJ/mol and −22 kJ/mol (Table 4), which are attributed to the physical adsorption (enthalpy change is in the range of −20−40 kJ/mol[71]).

Table 4. Estimated Values of Energy of Adsorption (Based on Langmuir Parameters and the Kinetic Theory of Gases

sample description	ΔH_{ad}, kJ/mol	ΔG^0_{ad}, kJ/mol
18 ft intact	−16.38	−34.65
18 ft powder	−14.89	−35.27
AB 9 ft intact	−17.99	−33.14
AB 9 ft powder	−18.68	−31.98
Big Pit intact	−19.36	−32.8
Big Pit powder	−21.91	−30.64

The Gibbs free energy of CO_2 adsorption on coal was calculated and is shown in Table 4. The adsorption energy/Gibbs free energy of adsorption are molar quantities that increase with the number of moles adsorbed. The findings were directly compared with previously reported findings on an 86% carbon content coal, where the enthalpy of adsorption ranged from 25.3 to 27.3 kJ/mol,[72] which is comparable with the current study's estimated values. The adsorption energy calculated in this work is similar to the numerical values of the heat of condensation of CO_2 (15.8 kJ/mol[73]), indicating that liquid-like adsorption theories such as BET should be used to explain CO_2 adsorption on coal.

4.2.2. Evaluation of CO_2 Adsorption on Coal Using Brunauer−Emmet−Teller (BET) Model. Figure 3a−c shows plots comparing experimental data from intact and powdered samples of 9 ft AB, 18 ft AB, and BP to results from the BET model. The BET model fitted the experimental data well (Figure 3a−c), indicating multilayer CO_2 adsorption on coal surfaces. Table 5 provides a summary of the BET parameters of the coal samples.

The monolayer coverage, N_m, values show that the inflection point occurred well below 1.0 MPa (Figure 3a−c; Table 5). This could be the reasons that the intermediate pressure experiments

https://doi.org/10.1021/acsomega.2c07940
ACS Omega XXXX, XXX, XXX−XXX

Table 5. Brunauer–Emmet–Teller (BET) Parameters of CO_2 Adsorption on Coal Samples

sample description	BET dimensionless parameter, c	adsorbed amount at monolayer coverage, N_m, g of CO_2/kg of coal	R^2 and (standard error of estimate)	specific surface area, m^2/kg	$Q_1 - Q_2$, (kJ/mol)[a]
18 ft AB intact	150	21.96	0.98 (6.6)	78408	12.42
18 ft AB powder	222	25.17	−0.2 (42)	89869	13.39
9 ft AB intact	52.95	32.79	0.91(6.5)	121397	9.839
9 ft AB powder	209	42.87	0.87 (7.1)	153067	13.24
Big pit intact	93.5	24.16	0.91 (4.1)	86263	11.25
Big pit powder	296.45	22.80	0.48 (7.2)	81407	14.11

[a] $Q_1 - Q_2$ is the difference between the energy of adsorption of the first layer and the subsequent liquid layers.

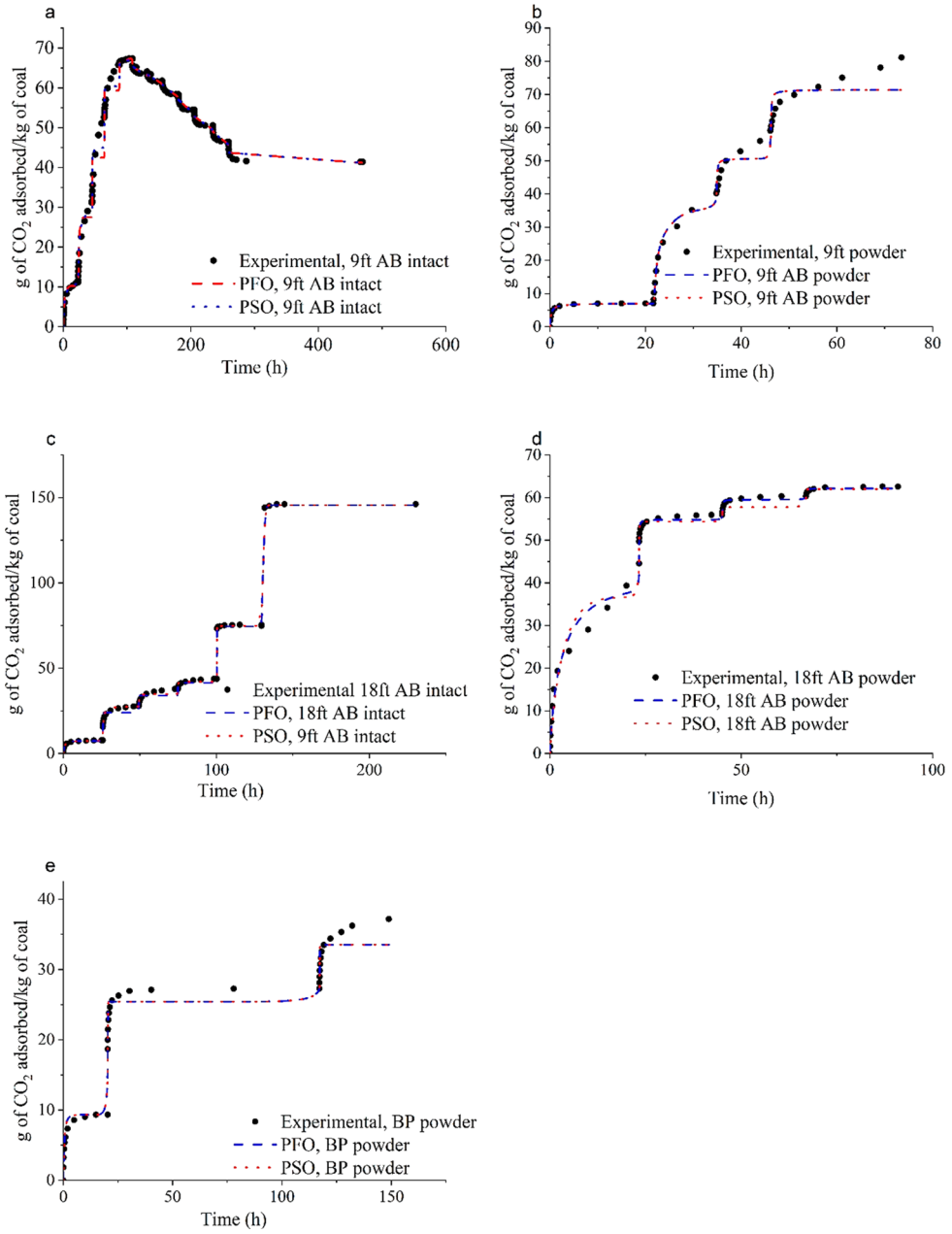

Figure 5. Experimental data fitted against the PFO and PSO model; (a) 9 ft AB intact, (b) 9 ft AB powder, (c) 18 ft AB intact, (d) 18 ft AB powder, and (e) Big Pit (BP) powder.

fit the BET model well where the liquid like adsorption occurs above the inflection point.

Q_1 kJ/mol (Table 5) is related to the energy of first layer adsorption (ΔH_{ad}). The magnitude of $Q_1 - Q_2$ is related to the

https://doi.org/10.1021/acsomega.2c07940
ACS Omega XXXX, XXX, XXX−XXX

Table 6. PSO and PFO Model Parameters Obtained for 9 ft AB Samples

		pseudo-first-order kinetics parameters			pseudo-second-order kinetics parameters		
	injection - equilibrium pressure (MPa)	equilibrium concentration (q_e) g of CO_2/kg of coal	rate constant, k_{a1} (h^{-1})	R^2 and standard error of estimate	equilibrium concentration (q_e) g of CO_2/kg of coal	rate constant k_{a2} (kg g^{-1} h^{-1})	R^2 and (standard error of estimate)
Powder	Adsorption						
	0.75−0.11	6.72	2.87	0.92 (0.49)	6.96	0.7	0.99 (0.19)
	1.51−0.73	34.26	1.07	0.85 (3.89)	37.99	0.04	0.99 (2.85)
	3−1.97	50.98	9.24	0.35 (4.65)	50.74	1.27	0.99 (4.67)
	4.51−3.5	69.71	37.13	0.2 (6)	71.42	0.92	0.42 (5)
Intact	Adsorption						
	0.56−0.07	10.46	0.52	0.96 (0.84)	11.52	0.058	0.99 (0.48)
	1.54−0.6	26.63	1.54	0.50 (5.12)	27.96	0.09	0.53 (5.29)
	3.03−1.86	44.99	4.86	0.25 (7.24)	47.94	0.14	0.7 (4.56)
	4.51−3.6	58.71	953	0.01 (4.80)	60.41	1.54	0.45 (3.80)
	Desorption		k_{d1} (h^{-1})				
	3.06−3.23	66.81	102	0.17 (0.24)	66.88	30.17	0.35 (0.26)
	1.87−2.38	65.43	0.002	0.51 (0.74)	65.44	2.79×10^{-5}	0.51 (0.74)
	1.53−1.89	66.39	0.002	0.66 (0.52)	63.4	2.54×10^{-5}	0.66 (0.52)
	1−1.4	60.89	0.002	0.76 (0.62)	60.9	3.63×10^{-5}	0.76 (0.61)
	0.6−0.99	57.06	0.0025	0.65 (0.86)	57.07	4.67×10^{-5}	0.66 (0.87)
	0.31−0.66	52.84	0.002	0.51 (0.99)	52.86	4.33×10^{-5}	0.52 (0.98)
	0.1−0.42	48.96	0.003	0.61 (0.84)	48.98	5.76×10^{-5}	0.62 (0.91)
	0−0.22	43.73	0.0002	0.33 (1.4)	48.98	6.85×10^{-5}	0.33 (1.4)

Table 7. PSO and PFO Model Parameters Obtained for 18 ft AB

		pseudo-first-order kinetics parameters			pseudo-second-order kinetics parameters		
	injection - equilibrium pressure (MPa)	q_e, equilibrium concentration, g of CO_2/kg of coal	rate constant, k_{a1} (h^{-1})	R^2 and standard error of estimate	q_e, equilibrium concentration, g of CO_2/kg of coal	rate constant k_{a2}, (kg g^{-1} h^{-1})	R^2 and (standard error of estimate)
Intact	0.58−0.08	7.25	1.21	0.95 (0.5)	7.75	0.23	0.99 (0.23)
	1.53−0.63	23.97	17.64	0.49 (3.06)	27.73	0.19	0.99 (1.26)
	3.04−2.02	33.37	31.57	0.25 (2.82)	37.83	1.68	0.60 (2.26)
	4.59−3.76	41.36	410.9	0.02 (1.7)	42.04	4.14	0.55 (1.24)
	5.52−4.99	74.47	346.91	0.92 (0.77)	74.82	9.5	0.99 (0.52)
	6.35−6.33	145.54	346	0.99 (0.81)	145.54	346	0.99 (0.81)
Powder	0.68−0.15	36.68	0.35	0.97 (4.18)	42.08	0.01	0.95 (3.08)
	1.65−0.77	54.39	52.93	0.99 (1.33)	54.85	3.48	0.91 (0.95)
	3.22−2.18	57.75	78.8	0.99 (1.59)	59.54	5.45	0.99 (0.61)
	4.5−3.67	61.96	74.77	0.99 (0.35)	62.14	9.92	0.99 (0.49)

heat of condensation or liquefaction of CO_2. The energy of adsorption values observed in the current study was comparable with the heat of condensation of CO_2 (approximately −16.7 kJ/mol[74]). This analysis indicates that CO_2 pore condensation occurs above the inflection point (>1 MPa; Figure 3a−c).

Table 5 summarizes the calculated available specific surface area on coal for the adsorption of gas molecules. The intact sample of bituminous BP coal (86263 m^2/kg) showed a higher surface area than the intact samples of anthracite 18 ft AB (78408 m^2/kg) and lower than the 9 ft AB (121397 m^2/kg) samples. The powdered samples of 9 ft AB had a higher specific surface area than the powdered samples of 18 ft AB and BP samples. The intact sample of BP (86263 m^2/kg) exhibited a similar specific microporous surface as the powdered samples of BP (81407 m^2/kg). This is effect of the bituminous coal structure (microporous porous network volume) on the adsorption of CO_2 in intact bituminous sample which resulted in a higher adsorption capacity. The obtained specific surface areas in the current work (78408 m^2/kg to 153067 m^2/kg) are comparable with the specific surface area available for CO_2 obtained by Zhao et al. (2016)[75] (77400 m^2/kg to 198400 m^2/kg).

4.2.3. Comparison of Langmuir and Brunauer− Emmet− Teller (BET) Models. To evaluate the adsorption of CO_2 by the coal samples, the Langmuir and BET models were compared based on the experimental data fitting effect. Nonlinear regression analysis has been used to fit the theoretical models and experimental results. The optimal model is shown by the combination of the correlation coefficient (R^2) and standard error of estimation (SEOE) (Tables 4 and 5). The BET model generally demonstrated good agreement with the experimental results for the intact samples. The experimental findings of powdered 18 ft AB and 9 ft AB anthracite samples fit the Langmuir model quite well. Both the BET and Langmuir models fit well with the experimental data of powder and intact samples of BP bituminous coal.

4.3. Kinetics of CO_2 Adsorption on Different Condition and Rank of Coal. Pseudo-first order (PFO) and pseudo-second order (PSO) kinetic models were used to fit the experimental data (that is, the amount adsorbed CO_2 versus time). The adsorbed CO_2 predicted by the PFO and PSO

https://doi.org/10.1021/acsomega.2c07940
ACS Omega XXXX, XXX, XXX−XXX

Table 8. PSO and PFO Model Parameters Obtained for Big Pit Coal

	pseudo-first-order kinetics parameters			pseudo-second-order kinetics parameters		
injection - equilibrium pressure (MPa)	q_e, equilibrium concentration, g of CO_2/kg of coal	rate constant, k_{a1}, h^{-1}	R^2 and standard error of estimate	q_e, equilibrium concentration, g of CO_2/kg of coal	rate constant k_{a2}, kg g^{-1} h^{-1}	R^2 and (standard error of estimate)
0.53−0.13	9.33	1.70	0.99 (0.88)	9.25	0.28	0.99 (0.39)
1.54−0.82	25.4	28.75	0.46 (1.73)	26.11	1.84	0.99 (1.13)
3.12−2.13	33.52	39.1	0.45 (2.12)	37.18	40.99	0.98 (4.5)

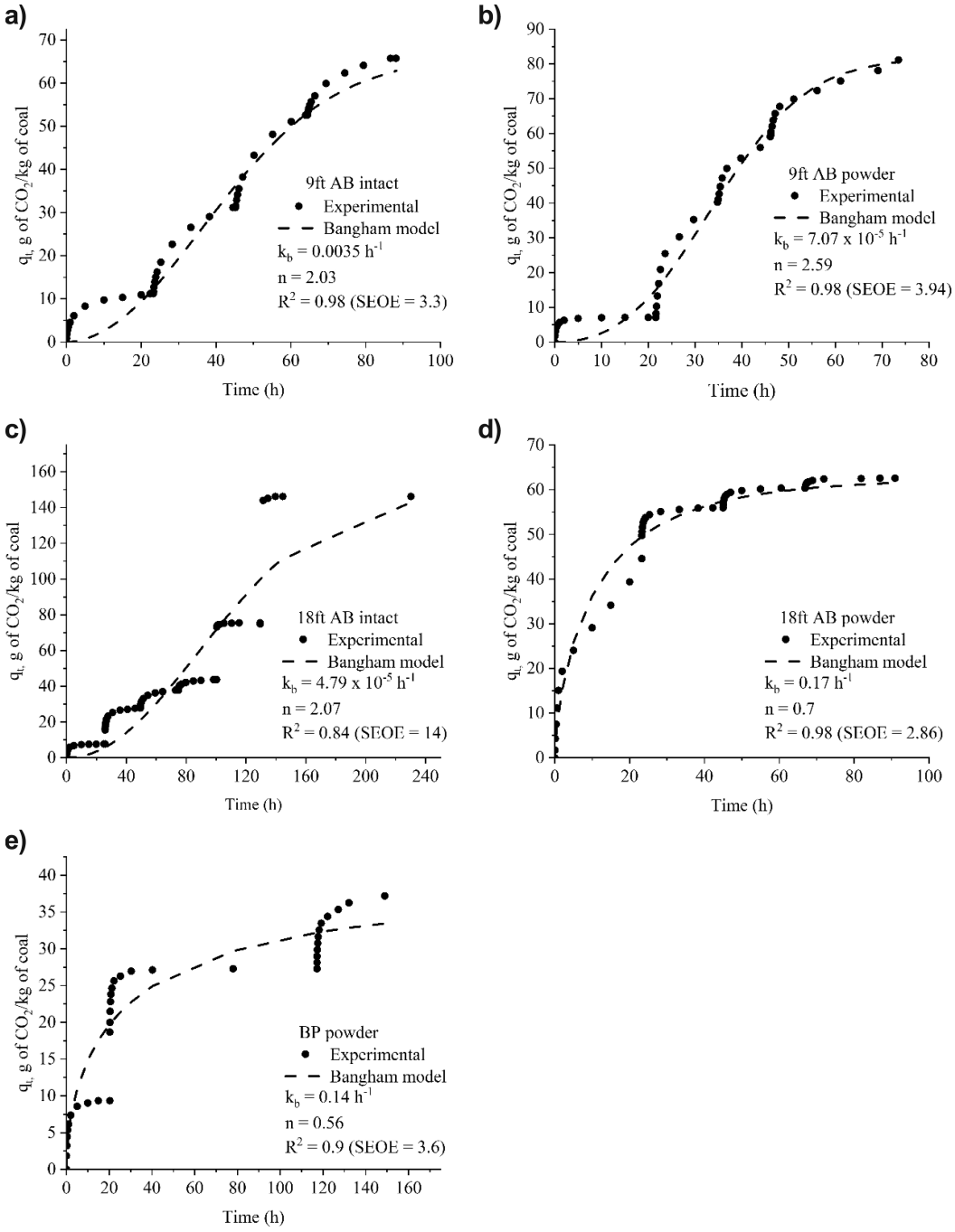

Figure 6. Bangham kinetic pore diffusion model fitting for (a) 9 ft AB intact (pressure range for up to 6.3 MPa), (b) 9 ft AB powder (pressure range for up to 6.3 MPa), (c) 18 ft AB intact (pressure range for up to 6.3 MPa), (d) 18 ft AB powder (pressure range for up to 6.3 MPa), and (e) BP powder (pressure range for up to 6.3 MPa).

models at time t (q_t, g adsorbed CO_2/kg coal) are plotted against the experimental values in Figure 5. Figure 5, panels a−e shows the results obtained for samples of 9 ft AB intact, 9 ft AB powder, 18 ft AB intact, 18 ft AB powder, and Big Pit powder, respectively. Tables 6, 7, and 8 show the rate constants (K_{ad1}, K_{ad2} for adsorption, and K_{de1} for desorption), equilibrium

https://doi.org/10.1021/acsomega.2c07940
ACS Omega XXXX, XXX, XXX−XXX

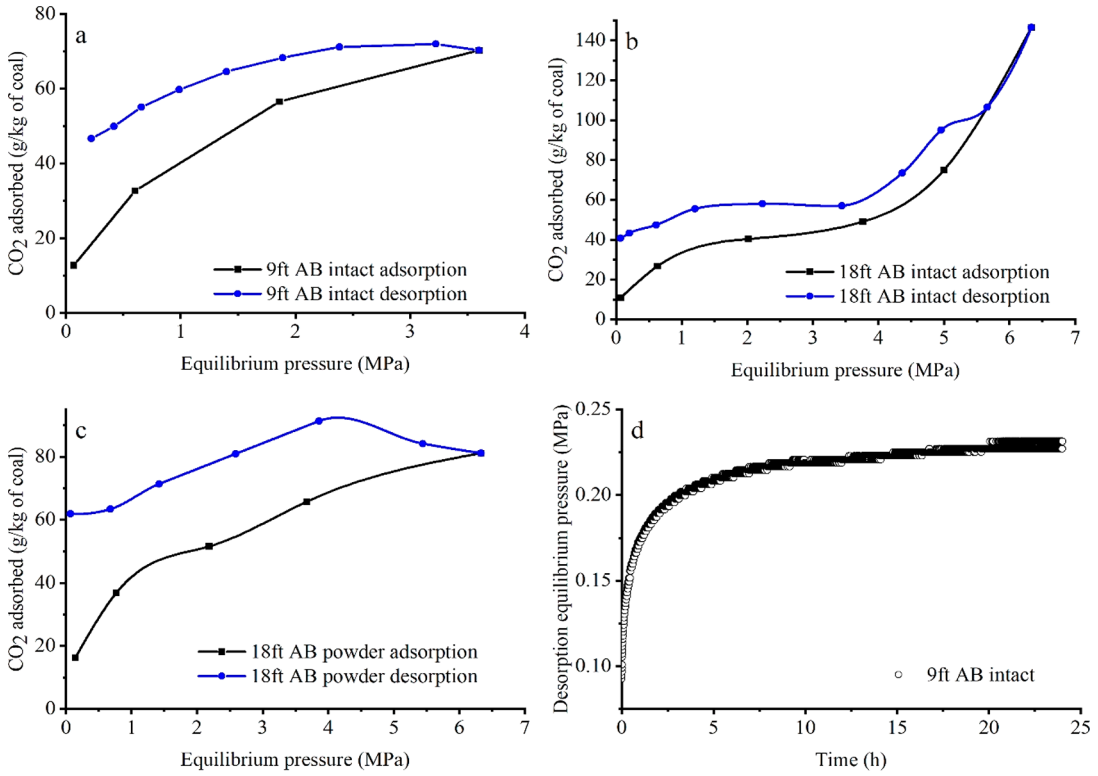

Figure 7. CO_2 adsorption and desorption behavior of (a) intact 9 ft Aberpergwm coal, (b) intact 18 ft Aberpergwm coal, (c) powdered 18 ft Aberpergwm, (d) pressure versus time curves observed for intact 9 ft AB sample after evacuating the sample to 0 MPa at 298.15 K.

concentration (q_e), standard error of estimate and R^2 values for the model fit for the 9 ft AB intact, 9 ft AB powder, 18 ft AB dry intact, 18 ft AB powder, and Big Pit powder, respectively.

Overall, the plots and the combination of standard error of estimate and correlation coefficient (R^2) indicate that the adsorption kinetics data agree well with the PSO model than the PFO model. The PSO model implies that surface interaction and bulk pore diffusion dominate CO_2 adsorption on coal.[76,77] The pressure dependence of K_{ad2} demonstrated that the pore diffusion being the rate-determining step in the beginning and surface interaction being the slowest rate-determining step at higher pressures (K_{ad1}, K_{ad2} values in Tables 6−8). There are only a few other studies to compare the kinetic parameters with. Gabruś et al. (2021)[78] published an experimental study on CO_2 adsorption on bituminous coal in which the results have been fitted into PFO and PSO models. The K_{ad1} and K_{ad2} values obtained at 298.15 K and 2 MPa equilibrium pressure were much higher than the values obtained in the current study. K_{ad1} was in the range of 1613×10^3 to 1011×10^3 h^{-1}, and K_{ad2} was in the range of 5752×10^3 h^{-1} to 11851×10^3 h^{-1}. However, these experiments were conducted for less than 24 h equilibrium time to reach the maximum pressure range of 2 MPa whereas the current study allowed the equilibrium to occur for each pressure steps (0.5 to 6.4 MPa).

Pore diffusion was more pronounced during the desorption kinetics, which fits both the PFO and PSO models well. The rate-limiting step in the desorption process was the slow release of CO_2 molecules trapped in the pores (K_{de1} values; Table 6). It can be seen from the results presented in Figure 5a that the adsorption−desorption kinetics plots of 9 ft AB intact, the model plot fitted very well with PFO model implying that the rate of desorption depends on the CO_2 trapped in the pores.

In order to explore whether the CO_2 adsorption is influenced by the mass transport phenomena of pore diffusion, the adsorption experimental data of 9 ft AB the Bangham model were used (eq 19).[37,65] The Bangham model assumes that pore diffusion influences the kinetics of the adsorption process. Equation 19 presents the nonlinear form of the model. The correlation coefficient (R^2) from the best-fit indicates the pore diffusion and pressure dependency of the constants k_b (h^{-1}), and n indicates the rate-determining step at the corresponding pressure range. The kinetic data acquired for the intact and powdered samples of 9 ft AB 18 ft AB, and powdered samples of BP were fitted with the model. Figure 6, panels a−e presents results for 9 ft AB intact, 9 ft AB powder, 18 ft AB intact, 18 ft AB powder, and Big Pit powder, respectively.

The higher correlation coefficient (R^2) in Figure 6a−e show that the pore diffusion is one of the rate determining steps. The correlation coefficient (R^2) value obtained for high pressure experiments up to 6.3 MPa for 18 ft AB coal was 0.84 (Figure 6c), which was less than the values obtained for lower pressure experiments for 18 ft AB powder (R^2 = 0.98; Figure 6d), 9 ft AB intact (R^2 = 0.98; Figure 6a), 9 ft AB powder (R^2 = 0.98; Figure 6b), and Big Pit powder (R^2 = 0.9; Figure 6e). These findings indicate that at lower pressures, bulk pore diffusion is the primary rate-determining step, while at higher pressures, surface interaction takes over, which is the slowest step.[79] Overall, the experimental data obtained from the current study fitted very well with the PSO kinetic model and Bangham pore diffusion model indicating that surface interaction and pore diffusion/condensation are the rate-determining steps in the CO_2 adsorption process on coal. The PSO model fit the data better than the Bangham model (based on R^2 and SEOE). However, the PSO model required separate segment fitting of each experimental pressure step up stage, whereas the Bangham

https://doi.org/10.1021/acsomega.2c07940
ACS Omega XXXX, XXX, XXX−XXX

model can use the entire data set without fitting each pressure step up stage separately.

4.4. Adsorption−Desorption Hysteresis. The adsorption and desorption isotherms of intact 9 ft AB, intact 18 ft AB, and powdered 18 ft AB coal samples are presented in Figure 7a,b,d. The positive deviation in the hysteresis indicates that some amount of CO_2 still adsorbed in the porous structure of the coal. This pattern also depicts the Type II and H3 adsorption−desorption pattern described by IUPAC classification for the pore diffusion/condensation dominated adsorption process.[70,80]

Adsorption hysteresis patterns differ between powder and intact samples of 18 ft AB for experiments up to 6.4 MPa, owing to high-density adsorbed phase formation in the intact coal fracture system and micropores. Comparatively the lower adsorption capacity observed with powdered 18 ft AB shows the effect of the physical nature of the intact sample and the effect of near critical pressure range (6.1 to 6.4 MPa; liquid and gas coexistence) CO_2 adsorption at 298.15 K (Figure 7b,c).

The adsorption−desorption hysteresis patterns were found to be consistent with previous work.[69,81−85] The current study experiments and findings reveal that the physical nature of coal and the thermodynamic nature of CO_2 provide a pathway to a deep pore matrix in which CO_2 molecules are trapped. Because CO_2 can enter through supermicropores (<2 nm), the ink bottle effect was observed in the hysteresis pattern of both intact and powdered samples.[29] As a result, the slow release of CO_2 trapped in the pores is observed as a positive deviation in the adsorption−desorption hysteresis pattern.

The amount of CO_2 that remained in the coal after the desorption experiments demonstrated the coal seams' ability to trap CO_2. The residual values for intact 9 ft AB, intact 18 ft AB, and powder 18 ft AB coal samples were 46.21 g/kg (1.05 mol/kg), 39.61 g/kg (0.9 mol/kg), and 51.93 g/kg (1.18 mol/kg), respectively. The higher residual amount of CO_2 adsorbed for the powdered sample for the 18 ft AB was attributed to the adsorption of CO_2 in the exposed (when the samples are powdered) super micropores (<2 nm) and evidence of ink bottle effect.[83] Figure 7d shows pressure versus time curves observed for intact 9 ft AB sample after evacuating the whole adsorption system to create null equilibrium pressure (0 MPa) at 298.15 K indicating the CO_2 entrapment in the pores.

The reversibility of CO_2 and the adsorption desorption hysteresis pattern are influenced by the sample type (intact and powdered) and coal rank. The hysteresis index (HI) values were calculated for 9 ft AB and 18 ft AB coal samples to evaluate the adsorption−desorption as described in Wang et al. (2014)[86] and Wang et al. (2016).[87] The adsorption desorption is completely reversible when HI = 0 and irreversible when HI = 1. Comparing the anthracite 18 ft AB intact and powder, the powder sample showed higher HI values (0.92) than that of intact samples (0.16). However, the low carbon content intact anthracitic sample (9 ft AB) had HI = 0.70. The carbon content is related to the coal rank and pore structure reflected on the desorption pattern. The higher HI (0.92) obtained for the higher rank powdered anthracitic 18 ft AB showed that the nanopores are exposed to CO_2 to enter when powdered indicating the sample physical type plays critical role in the desorption patten.

5. CONCLUSIONS

The adsorption−desorption isotherm patterns and kinetics of powdered and intact specimens of anthracite (9 ft AB and 18 ft AB) and bituminous (BP) coals obtained at the subcritical pressure range (up to 6.4 MPa) of CO_2 at temperature of 298.15 K using the manometric/volumetric adsorption measurement method were presented in this study.

- The CO_2 adsorption capacity of powdered samples of anthracite samples showed a higher adsorption capacity than that of intact samples due to the increased surface area which exposes the polarizing sites of anthracite coal and the nanopores.
- The intact bituminous (BP) coal showed a similar adsorption capacity as the powdered samples. Pulverizing the sample destroys the microfracture channel-like network that is specific to bituminous coals, and the results observed in this study demonstrated the effect of different porous networks of anthracite and bituminous coal samples on the CO_2 adsorption capacity.
- The experiments conducted at the near critical region (up to 6.4 MPa) showed that the intact samples exhibited a type II adsorption isotherm pattern with an upward trend, and the powdered sample showed a monolayer type plateau indicating the sample's physical nature had an impact on the type of the isotherm that occurs.
- Overall, the fitting of the adsorption experimental data and the theoretical model in this paper show that the BET model fits better than the Langmuir model.
- Within the coal rank, the reversibility of the CO_2 and hysteresis pattern were affected by the sample type (intact and powder). The powdered samples of anthracitic sample showed a higher degree CO_2 irreversibility than the intact sample indicating the CO_2 entrapment in the exposed nanopores. The analysis indicated that the experiments with large undisturbed samples are needed to test the adsorption capacity of specific coal type. The experimental results were fitted to PFO, PSO, and Bangham pore diffusion kinetic models, which showed that surface interaction and pore diffusion mechanisms are the rate-determining mechanisms of CO_2-coal adsorption processes.

Overall, the paper explored the effect of physical nature and subcritical pressure adsorption of CO_2 at 298.15 K in the context of CO_2 sequestration in shallow level coal seams.

AUTHOR INFORMATION

Corresponding Author

Maram Almolliyeh − *Geoenvironmental Research Centre (GRC), School of Engineering, Cardiff University, Cardiff CF24 3AA, United Kingdom;* orcid.org/0000-0002-3263-0555; Email: almolliyehm1@cardiff.ac.uk

Authors

Snehasis Tripathy − *Geoenvironmental Research Centre (GRC), School of Engineering, Cardiff University, Cardiff CF24 3AA, United Kingdom*

Sivachidambaram Sadasivam − *Geoenvironmental Research Centre (GRC), School of Engineering, Cardiff University, Cardiff CF24 3AA, United Kingdom;* orcid.org/0000-0002-2305-0292

Shakil Masum − *Geoenvironmental Research Centre (GRC), School of Engineering, Cardiff University, Cardiff CF24 3AA, United Kingdom*

Hywel Rhys Thomas − *Geoenvironmental Research Centre (GRC), School of Engineering, Cardiff University, Cardiff CF24 3AA, United Kingdom*

https://doi.org/10.1021/acsomega.2c07940
ACS Omega XXXX, XXX, XXX−XXX

Complete contact information is available at:
https://pubs.acs.org/10.1021/acsomega.2c07940

Notes

The authors declare no competing financial interest.

■ ACKNOWLEDGMENTS

The research was performed as part of the Sêr Cymru-Low Carbon Energy and Environment Research Network Wales project, which was partly funded by the European Regional Development Fund, through the Welsh Government. The authors are thankful to the funding agency. The authors are grateful to our research technicians Anthony Oldroyd and Malcolm Seaborne for their time and effort to run the high-pressure adsorption experiments. We appreciate Steven Rankmore, our technician, for extracting coal core samples.

■ REFERENCES

(1) White, C. M.; Smith, D. H.; Jones, K. L.; Goodman, A. L.; Jikich, S. A.; Lacount, R. B.; Dubose, S. B.; Ozdemir, E.; Morsi, B. I.; Schroeder, K. T. Sequestration of Carbon Dioxide in Coal with Enhanced Coalbed Methane Recovery: A Review. *Energy Fuels* **2005**, *19* (3), 659

(2) Zhou, W.; Wang, H.; Zhang, Z.; Chen, H.; Liu, X. Molecular Simulation of $CO_2/CH_4/H_2O$ Competitive Adsorption and Diffusion in Brown Coal. *RSC Adv.* **2019**, *9* (6), 3004−3011.

(3) Jones, E. J. P.; Voytek, M. A.; Warwick, P. D.; Corum, M. D.; Cohn, A.; Bunnell, J. E.; Clark, A. C.; Orem, W. H. Bioassay for Estimating the Biogenic Methane-Generating Potential of Coal Samples. *Int. J. Coal Geol.* **2008**, *76* (1−2), 138−150.

(4) Strapoć, D.; Mastalerz, M.; Eble, C.; Schimmelmann, A. Characterization of the Origin of Coalbed Gases in Southeastern Illinois Basin by Compound-Specific Carbon and Hydrogen Stable Isotope Ratios. *Org. Geochem.* **2007**, *38* (2), 267−287.

(5) Zhang, D.; Li, S.; Cui, Y.; Song, W.; Lin, W. Displacement Behavior of Methane Adsorbed on Coal by CO_2 Injection. *Ind. Eng. Chem. Res.* **2011**, *50* (14), 8742−8749.

(6) Kuuskraa, V. A.; Wicks, D. E.; Thurber, J. L. Geologic and Reservoir Mechanisms Controlling Gas Recovery From the Antrim Shale. *SPE Annu. Technol. Conf. Exhib.*; Washington, D.C., 1992; DOI: 10.2118/24883-ms

(7) Vangkilde-Pedersen, T.; Anthonsen, K. L.; Smith, N.; Kirk, K.; neele, F.; van der Meer, B.; Le Gallo, Y.; Bossie-Codreanu, D.; Wojcicki, A.; Le Nindre, Y. M.; Hendriks, C.; Dalhoff, F.; Peter Christensen, N. Assessing European Capacity for Geological Storage of Carbon Dioxide−the EU GeoCapacity Project. *Energy Procedia* **2009**, *1* (1), 2663−2670.

(8) Masoudian, M. S.; Airey, D. W.; El-Zein, A. Experimental Investigations on the Effect of CO_2 on Mechanics of Coal. *Int. J. Coal Geol.* **2014**, *128*−*129*, 12−23.

(9) Qin, C.; Jiang, Y.; Zuo, S.; Chen, S.; Xiao, S.; Liu, Z. Investigation of Adsorption Kinetics of CH_4 and CO_2 on Shale Exposure to Supercritical CO_2. *Energy* **2021**, *236*, 121410.

(10) Krooss, B. M.; Van Bergen, F.; Gensterblum, Y.; Siemons, N.; Pagnier, H. J. M.; David, P. High-Pressure Methane and Carbon Dioxide Adsorption on Dry and Moisture-Equilibrated Pennsylvanian Coals. *Int. J. Coal Geol.* **2002**, *51*, 69.

(11) Fitzgerald, J. E.; Pan, Z.; Sudibandriyo, M.; Robinson, R. L., Jr.; Gasem, K. A. M.; Reeves, S. Adsorption of Methane, Nitrogen, Carbon Dioxide and Their Mixtures on Wet Tiffany Coal. *Fuel* **2005**, *84*, 2351.

(12) Siemons, N.; Busch, A. Measurement and Interpretation of Supercritical CO_2 Sorption on Various Coals. *Int. J. Coal Geol.* **2007**; pp 229−242. DOI: 10.1016/j.coal.2006.06.004.

(13) Lee, H. H.; Kim, H. J.; Shi, Y.; Keffer, D.; Lee, C. H. Competitive Adsorption of CO_2/CH4Mixture on Dry and Wet Coal from Subcritical to Supercritical Conditions. *Chem. Eng. J.* **2013**, *230*, 93−101.

(14) De Silva, P. N. K.; Ranjith, P. G. Understanding and Application of CO_2 Adsorption Capacity Estimation Models for Coal Types. *Fuel* **2014**, *121*, 250−259.

(15) Li, D.; Liu, Q.; Weniger, P.; Gensterblum, Y.; Busch, A.; Krooss, B. M. High-Pressure Sorption Isotherms and Sorption Kinetics of CH_4 and CO_2 on Coals. *Fuel* **2010**, *89* (3), 569−580.

(16) Chen, S.; Tang, D.; Tao, S.; Xu, H.; Zhao, J.; Fu, H.; Ren, P. In-Situ Stress, Stress-Dependent Permeability, Pore Pressure and Gas-Bearing System in Multiple Coal Seams in the Panguan Area, Western Guizhou, China. *J. Nat. Gas Sci. Eng.* **2018**, *49*, 110−122.

(17) Masum, S. A.; Chen, M.; Hosking, L. J.; Stańczyk, K.; Kapusta, K.; Thomas, H. R. A Numerical Modelling Study to Support Design of an In-Situ CO_2 Injection Test Facility Using Horizontal Injection Well in a Shallow-Depth Coal Seam. *Int. J. Greenh. Gas Control* **2022**, *119*, DOI: 10.1016/j.ijggc.2022.103725.

(18) Day, S.; Fry, R.; Sakurovs, R. Swelling of Australian Coals in Supercritical CO_2. *Int. J. Coal Geol.* **2008**, *74* (1), 41−52.

(19) Mastalerz, M.; Gluskoter, H.; Rupp, J. Carbon Dioxide and Methane Sorption in High Volatile Bituminous Coals from Indiana, USA. *Int. J. Coal Geol.* **2004**, *60* (1), 43−55.

(20) Sadasivam, S.; Masum, S.; Chen, M.; Stańczyk, K.; Thomas, H. Kinetics of Gas Phase CO_2 Adsorption on Bituminous Coal from a Shallow Coal Seam. *Energy Fuels* **2022**, *36* (15), 8360−8370.

(21) Bachu, S. Screening and Selection Criteria, and Characterisation Techniques for the Geological Sequestration of Carbon Dioxide (CO_2). *Dev. Innov. Carbon Dioxide (Co* **2010**, *2*, 27−56.

(22) Elliott, J. R.; Lira, C. T. *Introductory Chemical Engineering Thermodynamics*. Prentice Hall: 2012, 2nd Edition.

(23) Pone, J. D. N.; Halleck, P. M.; Mathews, J. P. Sorption Capacity and Sorption Kinetic Measurements of CO_2 and CH_4 in Confined and Unconfined Bituminous Coal. *Energy Fuels* **2009**, *23* (9), 4688−4695.

(24) Espinoza, D. N.; Vandamme, M.; Pereira, J. M.; Dangla, P.; Vidal-Gilbert, S. Measurement and Modeling of Adsorptive-Poromechanical Properties of Bituminous Coal Cores Exposed to CO_2: Adsorption, Swelling Strains, Swelling Stresses and Impact on Fracture Permeability. *Int. J. Coal Geol.* **2014**, *134*−*135*, 80−95.

(25) Zagorščak, R.; Thomas, H. R. High-Pressure CO_2 Excess Sorption Measurements on Powdered and Core Samples of High-Rank Coals from Different Depths and Locations of the South Wales Coalfield. *Energy Fuels* **2019**, *33* (7), 6515−6526.

(26) Xu, H.; Tang, D.; Zhao, J.; Li, S.; Tao, S. A New Laboratory Method for Accurate Measurement of the Methane Diffusion Coefficient and Its Influencing Factors in the Coal Matrix. *Fuel* **2015**, *158*, 239−247.

(27) Tan, Y.; Pan, Z.; Liu, J.; Kang, J.; Zhou, F.; Connell, L. D.; Yang, Y. Experimental Study of Impact of Anisotropy and Heterogeneity on Gas Flow in Coal. Part I: Diffusion and Adsorption. *Fuel* **2018**, *232*, 444−453.

(28) Lu, X.; Armstrong, R. T.; Mostaghimi, P. Analysis of Gas Diffusivity in Coal Using Micro-Computed Tomography. *Fuel* **2020**, *261*, 116384.

(29) Li, Y.; Wang, Z.; Tang, S.; Elsworth, D. Re-Evaluating Adsorbed and Free Methane Content in Coal and Its Ad- and Desorption Processes Analysis. *Chem. Eng. J.* **2022**, *428*, 131946.

(30) Li, Y.; Wang, Y.; Wang, J.; Pan, Z. Variation in Permeability during CO_2−CH_4 Displacement in Coal Seams: Part 1 − Experimental Insights. *Fuel* **2020**, *263*, 116666.

(31) Li, Y.; Wang, J.; Wang, Z.; Pan, Z. Variation in Permeability during CO_2-CH_4 Displacement in Coal Seams. Part 2: Modeling and Simulation. *ACS Omega* **2020**, *5* (29), 18432−18440.

(32) Ren, J.; Weng, H.; Li, B.; Chen, F.; Liu, J.; Song, Z. The Influence Mechanism of Pore Structure of Tectonically Deformed Coal on the Adsorption and Desorption Hysteresis. *Front. Earth Sci.* **2022**, *10*. DOI: 10.3389/feart.2022.841353.

(33) Majewska, Z.; Ceglarska-Stefańska, G.; Majewski, S.; Zietek, J. Binary Gas Sorption/Desorption Experiments on a Bituminous Coal: Simultaneous Measurements on Sorption Kinetics, Volumetric Strain and Acoustic Emission. *Int. J. Coal Geol.* **2009**, *77* (1−2), 90−102.

(34) Shi, F.; Wei, Z.; Zhang, D.; Huang, G. Isotherms and Kinetics of Deformation of Coal during Carbon Dioxide Sequestration and Their Relationship to Sorption. *Int. J. Coal Geol.* **2020**, *231*, 103606.
(35) Hou, X.; Liu, S.; Zhu, Y.; Yang, Y. Experimental and Theoretical Investigation on Sorption Kinetics and Hysteresis of Nitrogen, Methane, and Carbon Dioxide in Coals. *Fuel* **2020**, *268*, 117349.
(36) Njikam, E.; Schiewer, S. Optimization and Kinetic Modeling of Cadmium Desorption from Citrus Peels: A Process for Biosorbent Regeneration. *J. Hazard. Mater.* **2012**, *213-214*, 242−248.
(37) Swan, E.; Urquhart, A. R. Adsorption Equations. *J. Phys. Chem.* **1927**, *31* (2), 251−276.
(38) British Standards Institution; British Standards Institution. Methods for Analysis and Testing of Coal and Coke. Part 104. Proximate Analysis. Section 104.3. Determination of Volatile Matter Content, 1998, 7.
(39) British Standards Institution; British Standards Institution. Methods for Analysis and Testing of Coal and Coke. Part 104. Proximate Analysis. Section 104.4. Determination of ash, 1998.
(40) British Standards Institution; British Standards Institution. Methods for Analysis and Testing of Coal and Coke. Part 104. Proximate Analysis. Section 104.1. Determination of moisture content of the general analysis tests sample, 1999.
(41) British Standards Institution; Methods for analysis and testing of coal and coke. Part 106. Ultimate analysis of coal and coke.Section 106.1.1. Determination of carbon and hydrogen content. High temperature combustion method, 1996.
(42) British Standards Institution.; Methods for analysis and testing of coal and coke. Part 106. Ultimate analysis of coal and coke.Section 106.4.2. Determination of total sulfur content. High temperature combustion method, 1996.
(43) *ASTM D3302 - Standard Test Method for Total Moisture in Coal, Engineering 360*, https://standards.globalspec.com/std/1033962/ASTM.
(44) Perry, S.; Perry, R. H.; Green, D. W.; Maloney, J. O. *Perry's Chemical Engineers' Handbook*; 2000; Vol. *38*. DOI: 10.5860/choice.38-0966.
(45) *ASTM D388-99 - Standard Classification of Coals by Rank*, https://webstore.ansi.org/standards/astm/astmd38899.
(46) Sudibandriyo, M.; Pan, Z.; Fitzgerald, J. E.; Robinson, R. L.; Gasem, K. A. M. Adsorption of Methane, Nitrogen, Carbon Dioxide, and Their Binary Mixtures on Dry Activated Carbon at 318.2 K and Pressures up to 13.6 MPa. *Langmuir* **2003**, *19*, 5323.
(47) Keller, J. U.; Staudt, R. Gas Adsorption Equilibria: Experimental Methods and Adsorptive Isotherms. *Gas Adsorpt. Equilibria Exp. Methods Adsorpt. Isotherms* **2005**, 1−422.
(48) Myers, A. L.; Monson, P. A. Physical Adsorption of Gases: The Case for Absolute Adsorption as the Basis for Thermodynamic Analysis. *Adsorption* **2014**, *20* (4), 591−622.
(49) ASTM International, ASTM D4892-14(2019)E1 - Standard Test Method for Density of Solid Pitch (Helium Pycnometer Method), Engineering 360.
(50) Tóth, J. Adsorption : Theory, Modeling, and Analysis. Marcel Dekker Edition: 2002, 1st edition.
(51) Span, R.; Wagner, W. A New Equation of State for Carbon Dioxide Covering the Fluid Region from the Triple-Point Temperature to 1100 K at Pressures up to 800 MPa. *J. Phys. Chem. Ref. Data* **1996**, *25* (6), 1509−1596.
(52) Gmehling, J.; Kleiber, M.; Kolbe, B.; Rarey, J. Chemical Thermodynamics for Process Simulation. Wiley-VCH Verlag GmbH: Germany, 2019, 2nd Edition.
(53) Langmuir, I. The Constitution and Fundamental Properties of Solids and Liquids. Part I. Solids. *J. Am. Chem. Soc.* **1916**, *38* (11), 2221−2295.
(54) Langmuir, I. The Constitution and Fundamental Properties of Solids and Liquids. II. Liquids. *J. Am. Chem. Soc.* **1917**, *39* (9), 1848−1906.
(55) Langmuir, I. The Adsorption of Gases on Plane Surfaces of Glass, Mica and Platinum. *J. Am. Chem. Soc.* **1918**, *40* (9), 1361−1403.
(56) Butt, H.; Graf, K.; Kappl, M. Physics and Chemistry of Interfaces. *Phys. Chem. Interfaces* **2003**, DOI: 10.1002/3527602313.
(57) Rouquerol, F.; Rouquerol, J.; Sing, K. Introduction. In *Adsorption by Powders and Porous Solids*; Academic Press, 1999; pp 1−26. DOI: 10.1016/b978-012598920-6/50002-6.
(58) Ruthven, D. M. Physical Adsorption and the Characterization of Porous Adsorbents. *Princ. Adsorpt. Adsorpt. Process.* **1985**, *19*, 433.
(59) Brunauer, S.; Emmett, P. H.; Teller, E. Adsorption of Gases in Multimolecular Layers. *J. Am. Chem. Soc.* **1938**, *60* (2), 309−319.
(60) Yang, R. T. Adsorbents and Adsorption Isotherms. *Gas Sep. by Adsorpt. Process.* **1987**, 9−48.
(61) Tien, C. Adsorption Equilibrium Relationships, Isotherm Expressions, Their Determinations, and Predictions. *Introd. to Adsorpt.* **2019**, 23−85.
(62) Guo, J.; Zhai, Z.; Wang, L.; Wang, Z.; Wu, J.; Zhang, B.; Zhang, J. Dynamic and Thermodynamic Mechanisms of TFA Adsorption by Particulate Matter. *Environ. Pollut.* **2017**, *225*, 175−183.
(63) Hu, A.; Zhang, Y.; Xiong, P.; Yang, Y.; Liu, Z.Kinetic Characteristics and Modeling Comparison of Methane Adsorption on Gas Shale *Energy Sources, Part A* **2020**, DOI: 10.1080/15567036.2020.1849461.
(64) Bangham, D. H.; Burt, F. P. The Behaviour of Gases in Contact with Glass Surfaces. *Proc. R. Soc. London. Ser. A, Contain. Pap. a Math. Phys. Character* **1924**, *105* (732), 481−488.
(65) Bangham, D. H.; Sever, W. XCIII. An Experimental Investigation of the Dynamical Equation of the Process of Gas-Sorption. *London, Edinburgh, Dublin Philos. Mag. J. Sci.* **1925**, *49* (293), 935−944.
(66) Bangham, D. H.; Burt, F. P. Sorption of Ammonia and Carbon Dioxide by Glass. *J. Phys. Chem.* **1925**, *29* (2), 113−129.
(67) Pone, J. D. N.; Halleck, P. M.; Mathews, J. P. Methane and Carbon Dioxide Sorption and Transport Rates in Coal at In-Situ Conditions. *Energy Procedia* **2009**, *1*, 3121−3128.
(68) Zhao, Y.; Liu, S.; Elsworth, D.; Jiang, Y.; Zhu, J. Pore Structure Characterization of Coal by Synchrotron Small-Angle X-Ray Scattering and Transmission Electron Microscopy. *Energy Fuels* **2014**, *28* (6), 3704−3711.
(69) Harpalani, S.; Prusty, B. K.; Dutta, P. Methane/CO_2 Sorption Modeling for Coalbed Methane Production and CO_2 Sequestration. 2006. DOI: 10.1021/ef050434l.
(70) Sing, K. S. W.; Everett, D. H.; Haul, R. A. W.; Moscou, L.; Pierotti, R. A.; Rouquerol, J.; Siemieniewska, T. Reporting Physisorption Data for Gas/Solid Systems with Special Reference to the Determination of Surface Area and Porosity. *Pure Appl. Chem.* **1985**, *57* (4), 603−619.
(71) Atkins, P. W.; de Paula J, K. J. *Physical Chemistry*, 11th ed.; Oxford Univ. Press: Oxford, 2017; p 944.
(72) Ozdemir, E.; Schroeder, K. Effect of Moisture on Adsorption Isotherms and Adsorption Capacities of CO_2 on Coals. *Energy Fuels* **2009**, *23* (5), 2821−2831.
(73) Speight, D. J. G. *Lange's Handbook of Chemistry*; McGraw-Hill Education, 2017.
(74) *NIST Chemistry WebBook*, https://webbook.nist.gov/chemistry/. Accessed: 31-01-2022.
(75) Zhao, J.; Xu, H.; Tang, D.; Mathews, J. P.; Li, S.; Tao, S. A Comparative Evaluation of Coal Specific Surface Area by CO_2 and N2 Adsorption and Its Influence on CH4 Adsorption Capacity at Different Pore Sizes. *Fuel* **2016**, *183*, 420−431.
(76) Plazinski, W.; Dziuba, J.; Rudzinski, W. Modeling of Sorption Kinetics: The Pseudo-Second Order Equation and the Sorbate Intraparticle Diffusivity. *Adsorption* **2013**, *19* (5), 1055−1064.
(77) Tang, X.; Ripepi, N.; Gilliland, E. Isothermal Adsorption Kinetics Properties of Carbon Dioxide in Crushed Coal. *Greenh. Gases Sci. Technol.* **2016**, *6* (2), 260−274.
(78) Gabruś, E.; Wojtacha-Rychter, K.; Aleksandrzak, T.; Smoliński, A.; Król, M. The Feasibility of CO_2 Emission Reduction by Adsorptive Storage on Polish Hard Coals in the Upper Silesia Coal Basin: An Experimental and Modeling Study of Equilibrium, Kinetics and Thermodynamics. *Sci. Total Environ.* **2021**, *796*, 149064.

https://doi.org/10.1021/acsomega.2c07940
ACS Omega XXXX, XXX, XXX−XXX

(79) Tütem, E.; Apak, R.; Ünal, Ç. F. Adsorptive Removal of Chlorophenols from Water by Bituminous Shale. *Water Res.* **1998**, *32* (8), 2315−2324.
(80) Thommes, M.; Kaneko, K.; Neimark, A. V.; Olivier, J. P.; Rodriguez-Reinoso, F.; Rouquerol, J.; Sing, K. S. W. Physisorption of Gases, with Special Reference to the Evaluation of Surface Area and Pore Size Distribution (IUPAC Technical Report). *Pure Appl. Chem.* **2015**, *87* (9−10), 1051−1069.
(81) Busch, A.; Gensterblum, Y.; Krooss, B. M. Methane and CO_2 Sorption and Desorption Measurements on Dry Argonne Premium Coals: Pure Components and Mixtures. *Int. J. Coal Geol.* **2003**, *55*, 205.
(82) Ozdemir, E.; Morsi, B. I.; Schroeder, K. CO_2 Adsorption Capacity of Argonne Premium Coals. *Fuel* **2004**, *83* (7−8), 1085−1094.
(83) Pan, Z.; Connell, L. D.; Camilleri, M. Laboratory Characterisation of Coal Reservoir Permeability for Primary and Enhanced Coalbed Methane Recovery. *Int. J. Coal Geol.* **2010**, *82* (3−4), 252−261.
(84) Dutta, P.; Bhowmik, S.; Das, S. Methane and Carbon Dioxide Sorption on a Set of Coals from India. *Int. J. Coal Geol.* **2011**, *85* (3−4), 289−299.
(85) Mukherjee, M.; Misra, S. A Review of Experimental Research on Enhanced Coal Bed Methane (ECBM) Recovery via CO_2 Sequestration. *Earth-Science Rev.* **2018**, *179*, 392−410.
(86) Wang, K.; Wang, G.; Ren, T.; Cheng, Y. Methane and CO_2 Sorption Hysteresis on Coal: A Critical Review. *Int. J. Coal Geol.* **2014**, *132*, 60−80.
(87) Wang, G.; Da; Ren, T. X.; Qi, Q. X.; Wang, K.; Zhang, L. Mechanism of Adsorption-Desorption Hysteresis and Its Influence on Deep CBM Recovery. *Meitan Xuebao/Journal China Coal Soc.* **2016**, *41* (1), 49−56.

https://doi.org/10.1021/acsomega.2c07940
ACS Omega XXXX, XXX, XXX−XXX